# FEASIBILITY OF A COMPACT AXIAL FLOW
NUCLEAR HEAT EXCHANGER

Charles Anthony Kiser

77

FEASIBILITY OF A

COMPACT AXIAL FLOW NUCLEAR HEAT EXCHANGER

by

Charles Anthony Kiser

A Thesis Submitted to the

Graduate Faculty in Partial Fulfillment of

The Requirements for the Degree of

MASTER OF SCIENCE

Major Subject: Engineering

Approved:

TABLE OF CONTENTS

ABSTRACT

Computations indicate that when utilized in an idealized
ramjet at a flight Mach number of 2.5 and an altitude of
37,500 feet, a constant area axial flow nuclear heat exchanger
will be expected to produce 9,500 pounds of thrust with an air
inlet Mach number of 0.2, a weighted radial temperature aver-
age of 2000°F and a frontal area of 7.7 square feet. Molyb-
denum alloy with a disilicide coating was selected as the
container material. Sandwiched between the molybdenum was a
fissionable alloy of highly enriched uranium and zirconium.
From a nuclear aspect the unreflected heat exchanger becomes
critical at a diameter of 40 inches and a length of 60 inches
with a total weight of 8,052 pounds which includes 3,622
pounds of 90 per cent enriched uranium.

INTRODUCTION

That a constant-area axial-flow compact nuclear heat
exchanger as envisioned in Figure 1 when installed in an
idealized ramjet would produce significant thrust was the
basis of this thesis. Feasibility conclusions were limited
to the information revealed by heat transfer and nuclear
analysis under one assumed steady state condition. The
problems of nuclear control, shielding, thermal stresses,
and performance under different inlet Mach numbers were not
considered.

The nuclear heat exchanger as shown in Figure 2 incor-
porates thin concentric cylinders which are the solid fis-
sionable containers. The alloyed fissionable phase is
sandwiched between two layers of non-fissionable structural
material so that the enriched uranium fuel cores are sur-
rounded by a continuous network of structural metal for
strength and containment at high temperatures. Air flows
within the annuli and acts as the coolant and thrust agent.
It is recommended that the nuclear flux be flattened by a
central control core and a peripheral reflector; however, the
beneficial effects of a reflector and central control core
were not considered.

From the assumed inlet condition, various maximum cyl-
inder or wall temperatures were selected arbitrarily for
thrust results. That the high temperature fuel elements and

structural materials were possible metallurgically were next
investigated. Whether or not an unreflected homogeneous
reactor of this configuration can be made critical was deter-
mined by using one group diffusion theory.

LIST OF SYMBOLS

A   Cross section area normal to flow, (ft^2), or the mass
         number of an element (gm/gm atomic weight).

A_w Wetted area, (ft^2).

B   Buckling, (cm^{-2}).

c   Local velocity of sound, (ft/sec).

C_p Specific heat at constant pressure, (BTU/lb °F).

D   Diffusion coefficient for flux, (cm).

D_e Hydraulic diameter, $D_2 - D_1$, (ft).

D_1 Inside diameter, (ft).

D_2 Outside diameter, (ft).

$-D\nabla^2\phi$ Neutron leakage, $(n/cm^3\ sec)$.

f   Friction factor defined as $2g\ \tau_w/\rho v^2$.

g   Acceleration of gravity $(32.2\ ft/sec^2)$.

G   Mass velocity $(lb/sec\ ft^2)$.

h   Coefficient of heat transfer between fluid and surface,
         $(BTU/hr\ ft^2\ °F)$.

         h_e based on $(T_{o,w} - T_{o,aw})$.

         h_L based on logarithm mean of $(T_{o,w} - T)$.

         h_m based on $(T_{o,w} - T)$.

         h_s based on $(T_{o,w} - T_o)$.

H   Extrapolated distance, (cm).

k   Neutron multiplication factor.

K   Thermal conductivity, $(BTU/hr\ ft^2\ °F/ft)$.

L   Length of heat exchanger heating element in the longitudinal direction, (ft).

$\dot{m}$ Mass rate of flow, (lb/sec).

M   Mach number or molecular weight (gms/gm molecular weight).

n   Number of neutrons per cm^3.

N   Number of nuclei per cm^3.

N_0 Avogadros number (6.02×10^{23} nuclei/gm atomic weight).

N_{PR} Prandtl number, $C_p \mu / K$.

N_{RE} Reynolds number, $\rho v D_e / \mu$.

N_{ST} Stanton number, $h_e / C_p G$.

P   Absolute stream pressure (lb/in^2).

P_0 Isentropic stagnation pressure (lb/in^2).

q   Heat-transfer rate (BTU/hr).

Q   Volumetric heat source which is equal to $E \Sigma_f \phi$, (BTU/sec cm^3).

r   Radius (ft).

T   Absolute stream temperature (°R).

T_h Thrust (lb).

T_0 Stagnation temperature (°R).

$T_{0,aw}$ Adiabatic stagnation wall temperature (°R).

$T_{0,w}$ Stagnation wall temperature (°R).

v   Velocity (ft/sec).

V   Volume (ft^3 or cm^3).

W   Weight (lb).

x   Distance along heat exchanger heating elements (ft).

Subscripts

b	Bulk (T).
f	Film $t_f = (t_b + t_w)/2$.
w	Wall.
0,1,2	Station references

Greek

a	Definition of $\pi x/L$.
γ	Ratio of specific heats of gas, $C_p/C_v = 1.4$.
Δh	Change in enthalpy, (BTU/lb).
η	Number of neutrons produced per absorption in the fissionable isotope.
λ	Definition of $(N_{PR})_f^{-2/3}$.
λ_t	Transport mean free path, (cm).
μ	Absolute viscosity of the fluid, (lb/sec ft).
$\bar{\mu}_o$	Average cosine of the scattering angle per neutron collision in the laboratory system.
ν	Number of neutrons produced per fission in the fissionable isotope.
ρ	Density, (lb/ft^3).
σ	Microscopic cross section (cm^2).
	σ_a microscopic absorption cross section (cm^2).
	σ_s microscopic scattering cross section (cm^2).
	σ_f microscopic fission cross section (cm^2).

Σ Macroscopic cross section (cm^{-1}), ($N\sigma$).

         Σ_a macroscopic absorption cross section (cm^{-1}).

         Σ_s macroscopic scattering cross section (cm^{-1}).

         Σ_f macroscopic fission cross section (cm^{-1}).

$\Sigma_a\phi$ Number of neutron absorptions / cm^3 sec.

T_w Tractive force at wall due to fluid friction (lb/ft^2).

ϕ Flux in neutrons / cm^2 sec.

∇^2 Laplacian operator.

LIMITING CONDITIONS

To obtain a realistic operating condition for the air-cooled nuclear heat exchanger the following conditions were assumed:

$$M_0 = 2.5, \quad h = 37,500 \text{ ft}, \quad T = 392°R, \quad P = 3.09 \text{ lb/in}^2$$

Godsey and Young (1, p.221) stated that the total temperature through the inlet diffuser depends only on flight Mach number and ambient temperature and is a constant regardless of diffuser losses if the process is considered adiabatic. Therefore the relation

$$T_{0,0} = T_{0,1} = T_{0,2} = T(1 + \frac{\gamma-1}{2} M_0^2) \tag{1}$$

may be used where the station numbers correspond to those of Figure 1. Godsey and Young (1, p.221) stated that the total pressure at the heat exchanger inlet, $P_{0,2}$, was dependent upon the flight Mach number, ambient pressure, free stream diffusion losses, duct friction losses, and duct diffusion losses. The last three effects may be grouped under the term ram effectiveness or pressure recovery effectiveness. From data presented by Godsey and Young (1, p.86), the ram effectiveness at $M_0 = 2.5$ was given as approximately 0.98; however, subsonic diffusion was assumed to be loss free. For a more realistic condition a value of 0.90 was chosen. The above ratios may be

written out in the following expression for stagnation pressure at the heat exchanger inlet:

$$P_{0,2} = P_0(1 + \frac{\gamma - 1}{2} M_0^2)^{\gamma/\gamma - 1} \times \frac{P_{0,2} \text{ actual}}{P_{0,2} \text{ ideal}} \tag{1a}$$

Solutions to Equations 1 and 1a give $T_{0,2} = 884°R$ and $P_{0,2} = 46.5$ lb per sq in. for inlet conditions to the heat exchanger.

Prior to converting the above inlet stagnation pressure to stream pressure, it is necessary to examine the limiting conditions for heat exchange. Assuming a uniform cross sectional heat exchanger area under a given inlet stagnation temperature, which in this case is $884°R$, and various inlet Mach numbers, it is desired to exchange heat to the extent that the stagnation temperature at the exit of the heat exchanger be raised to a maximum value. By use of methods outlined in Reference (2, p.4.24) the results of various inlet Mach numbers are shown on Figure 3 which reveal that when a certain maximum temperature occurs, thermal choking even under frictionless conditions exists in the heating process and definitely limits the capacity of the constant area combustor or heat exchanger. Stated another way, if at any position downstream for a constant area duct, the stagnation temperature is equal to $T_{0,3}$ maximum, the flow is choked since the Mach number is unity. Any addition of friction

will reduce the downstream interval for $T_{0,3}$ maximum to occur. With $M_2 = 0.2$ and $T_{0,3}$ maximum achieved, 5100°R, the stagnation pressure would suffer a 20 per cent loss due entirely to the heating effect.

Without becoming involved with a specific shock cone and diffuser design, the inlet Mach number was set at 0.2, which resulted in the following stream conditions:

$$P_2 = 45.1 \text{ lb/in}^2$$
$$\rho_2 = .1385 \text{ lb/ft}^3$$
$$v_2 = 291 \text{ ft/sec}$$
$$T_2 = 880°R$$
$$G = 40.4 \text{ lb/ft}^2 \text{ sec}$$

As shown by Figure 2, the heat exchanger elements are thin hollow constant concentric area right cylinders which are adaptable to one-dimensional compressible gas flow treatment without introducing serious errors. This assumes that in any one annulus the change of stream properties in the direction of flow is much larger than in the radial direction.

HEAT TRANSFER ANALYSIS

McAdams (3, p.289) correlated the experimental data of Kays and London (4) and because compactness of an air-borne heat exchanger is an important parameter, a comparison of heat transfer coefficients per unit volume for a given friction power per unit volume showed ruffled fins and louvered plate fins as being the most effective. It appears that the highest ratio of heat transfer to pumping power is obtained when form drag is absent, or when all the drag is due to skin friction which is the case in common for flat plates or fins. Even though externally finned tubes are of value in increasing the rate of heat transfer, friction losses become prohibitive for this type of installation. For these reasons thin concentric hollow cylinders were chosen as the fuel elements of the heat exchanger and were restricted to constant longitudinal cross section area for nuclear simplification.

Development

If heat loss and longitudinal thermal conductivity are neglected, the rise in the enthalpy of the air per second is related to the effective coefficient of heat transfer from an annulus by a differential equation which is developed in Appendix C as

$$\frac{\pi}{4}(D_2{}^2 - D_1{}^2)\rho \, v \, C_p \, dT_0 = h_e \pi (D_2 + D_1)(T_{0,w} - T_{0,aw}) \, dx. \quad (2)$$

The particular temperature differential is shown schematically in Figure 4. The temperature increment for heat transfer is the difference between the actual wall temperature, $T_{0,w}$, and the temperature $T_{0,aw}$, which the wall would assume for the same flow conditions but with zero heat flux. McAdams et al. (5) found that the effective heat transfer coefficient, h_e, expressed in terms of the Stanton number, N_{ST}, was independent of the temperature potential, $T_{0,w} - T_0$, when based on $T_{0,w} - T_{0,aw}$ while the coefficients h_m and h_s were not independent.

The Reynolds analogy with $N_{PR} = 1$ relates the Stanton number to the friction factor by

$$\frac{h_e}{C_p G} = \frac{f}{2} \quad . \quad (3)$$

From experimental data for a moderate ΔT, $L/D_e = 60$, and $5,000 < N_{RE} < 200,000$, the following equations from McAdams (3, pp.155,219) may be combined

$$f = .046/(DG/\mu_f)^{.2} \quad (4)$$

$$\frac{h_L}{C_{pb} G}\left(\frac{C_p \mu}{K}\right)_f^{2/3} = \frac{.023}{(DG/\mu_f)^{.2}} \quad (5)$$

to produce

$$\frac{h_L}{c_{pb}G} = \frac{\lambda f}{2} \tag{6}$$

where, by definition, $\lambda \equiv (N_{PR})_f^{-2/3}$. Since Equations 3 and 6 are essentially the same, the limitation to a moderate temperature change may be removed without introducing serious errors when using the previously defined temperature potential. The following relationship, where specific heat is considered a constant, is used for the remainder of the analysis:

$$\frac{h_o}{c_p G} = \frac{\lambda f}{2} \tag{7}$$

The friction factor of Equation 7 is set by Equation 4 which is dependent upon Reynolds number and the degree of roughness. Since mass velocity, G, and specific heat are essentially constant, the friction factor may be considered to depend upon hydraulic diameter, viscosity, and degree of roughness. An average value of $\lambda f = .008$ was obtained from Equation 4 for $1/2" < D_e < 1\text{-}1/2"$ and $1400°R < \mu_f < 1600°R$. The variance of the friction factor within the above range of hydraulic diameter may be compensated for by added degrees of roughness; however, Cope (6) found that with water in the turbulent region even though friction was six times that for smooth pipes, the heat transfer was only 20 to 100 per cent greater than for smooth tubes. McAdams (3, p.223) states that because of a very

small temperature change the heat transfer coefficients ob-
tained were somewhat uncertain. Correlation with air may not
apply due to different Prandtl number effect; however, there
is a possibility that with small variation in hydraulic diam-
eter the friction factor could remain a constant by varying
the degrees of roughness.

Experimental data have shown that for turbulent flow in
rectangular ducts and annular spaces friction may be evaluated
from data for circular pipes using a hydraulic diameter shown
in Figure 2 as

$$D_e = 4r_h = \frac{\pi(D_2{}^2 - D_1{}^2)}{\pi(D_2 + D_1)} = D_2 - D_1 \quad . \quad (8)$$

A combination of Equations 2 and 7 with Equation 8 results in

$$\frac{d\,T_0}{T_0} = \frac{T_{0,w}}{T_0} - \frac{T_{0,aw}}{T_0} \quad 2\,\lambda f\,\frac{dx}{D_e} \quad . \quad (9)$$

If a gas stream of uniform temperature is brought to rest
isentropically, as at the stagnation of a blunt body, the tem-
perature rise for an ideal gas will be

$$T_0 - T = \frac{V^2}{2g\,JC_p} = T(1 + \frac{\gamma - 1}{2}\,M^2) \quad . \quad (10)$$

For convenience a temperature recovery factor N_{RF} as shown in
Figure 4 is defined as

$$N_{RF} \equiv \frac{T_{0,aw} - T}{T_0 - T} = \frac{T_{0,aw} - T}{V^2/2g\ JC_p} \qquad . \qquad (11)$$

By a combination of Equation 10 and 11, the stream temperature, T, may be eliminated to produce

$$\frac{T_{0,aw}}{T_0} = 1 - \frac{(1 - N_{RF})\ \frac{\gamma-1}{2}\ M^2}{1 + \frac{\gamma-1}{2}\ M^2} \qquad . \qquad (12)$$

Substitution of Equation 12 into 9, yields

$$\frac{dT_0}{T_0} = \left[\frac{T_{0,w}}{T_0} - 1 + \frac{(1 - N_{RF})\ \frac{\gamma-1}{2}\ M^2}{1 + \frac{\gamma-1}{2}\ M^2} \right] 2\lambda f\ \frac{dx}{D_e} \qquad . \qquad (13)$$

The generalized differential Mach number equation of Reference (2, p.4.12) simplifies to

$$\frac{dM^2}{M^2} = \frac{(1 + \gamma M^2)(1 + \frac{\gamma-1}{2}\ M^2)}{} \frac{dT_0}{T_0}$$

$$+ \frac{M^2(1 + \frac{\gamma-1}{2}\ M^2)}{1 - M^2}\ 4f\ \frac{dx}{D_e} \qquad (14)$$

with negligible structure drag forces and constant specific heat, molecular weight, area and mass flow rate.

$$(12) \qquad \ldots$$

$$(13) \qquad \ldots$$

$$(14) \qquad \ldots$$

$$(15) \qquad \ldots$$

Equation 13 was substituted into Equation 14 which gave

$$dM^2 = \frac{M^2(1 + \frac{\gamma -1}{2} M^2)}{1 - M^2} \; 2f \; \frac{dx}{D_e} \; .$$

$$\left\{ (1 + \sigma M^2)\lambda \left[\frac{T_{0,w}}{T_0} - 1 + \frac{1 - N_{RF} \frac{\gamma -1}{2} M^2}{1 + \frac{\gamma -1}{2} M^2} \right] + 2 \sigma M^2 \right\} \quad (15)$$

For a turbulent boundary layer over a flat plate, McAdams (3, p.311) recommends that the temperature recovery factor and the Prandtl number be related by

$$N_{RF} = N_{PR}^{1/3} \qquad . \qquad (16)$$

McAdams et al. (5) reported recovery factors for subsonic flow of air near the outlet and of a long smooth tube were in good agreement with those predicted by Equation 16. Appendix A shows the procedure for solving Equations 13 and 15 for one Mach number and stagnation temperature at an assumed position downstream. From these calculations it was evident that the contribution of the recovery factor term N_{RF}, was negligible for Mach numbers up to approximately 0.8; however, the resulting stagnation temperatures will be nearly 1.5 per cent higher than those which have incorporated this term.

For the remainder of this analysis the recovery factor and Prandtl number were assumed unity which reduced Equation 13 to

16

$$\frac{dT_0}{T_0} = \left[\frac{T_{0,w}}{T_0} - 1 \right] 2f \frac{dx}{D_e} \qquad (17)$$

It is of interest to note that Equation 17 could be expected from experimental data by McAdams (3, p.314) because the heat transfer coefficient, h_s, decreases and approaches the constant value of h_e for temperature differences greater than 100°F. For a high temperature potential, h_s approaches h_e and may be used directly in Equation 1.

Equations 14 and 17 were integrated approximately over short intervals of Mach numbers by using the procedure outlined in Reference (2, 4.60). Appendix B contains the stepwise procedure used and Tables 1-3, Appendix B, have the complete data for stagnation and stream properties as a function of L/D_e ratios for various longitudinally constant wall temperatures. Stagnation temperatures and pressures versus L/D_e ratios are shown in Figure 5.

However, from a nuclear standpoint the longitudinal flux of fuel element cylinders will follow a sine distribution with the maximum flux produced at the midpoint. This does not imply that the maximum wall temperature will occur at the longitudinal midpoint. By use of

$$T_{0,3} - T_{0,2} = \frac{2(T_{0,w\ max} - T_{0,2})}{1 - \sec \alpha\ max} \qquad (18)$$

which was developed in Appendix C and by using the previously
selected temperatures for maximum wall temperatures, the
stagnation temperatures versus L/D_e ratios were computed as
shown in Table 4 of Appendix C and plotted in Figure 5. Stag-
nation pressures for variable wall temperatures were obtained
by interpolation from previously calculated pressures.

An isentropic expansion using air data from Keenan and
Kaye (7) was assumed in order to obtain the change of enthalpy
from stage 3 to 4 of Figure 1. The Brayton cycle as shown in
Figure 6 represents an overall view; however, at various L/D_e
ratios, the change of enthalpy was computed using an ambient
pressure of 3.09 lb per sq in. Figure 7 shows the variance
of enthalpy for both constant and variable wall temperatures.
The right hand ordinate of Figure 7 related change of enthalpy
to pounds of thrust per sq ft by

$$\frac{T_h}{A} = \frac{G}{g} \ (v_4 - v_0) \qquad , \qquad (19)$$

where $v_0 = 2.5c$ and $v_4 = 223.7\sqrt{h_{0,3} - h_4}$.

Discussion

The calculated values of stagnation temperatures and
pressure as shown in Figure 5 do not show the contributing
effects on heat transfer and friction caused by the length

to diameter ratio and the effects of sudden enlargement or contraction of flow. The former effect is small since the L/D_e ratio for this heat exchanger should be greater than 60; the latter effect may still be appreciable even though the peripheral thickness of the cylinders are in the order of 0.05 to 0.07 in. The specific heat ratio was set at 1.4, and the friction factor, specific heat, and mass velocity were constant throughout the heating process. The cosine flux distribution in the longitudinal direction is justifiable for a finite cylinder.

The temperatures obtained by normal forced convection methods for an assumed $T_{0,w} = 2460°R$ are shown in Figure 5 for comparison. The temperatures show good correlation with stagnation temperatures obtained by the Reynolds analogy but are considerably higher than the stream temperatures. The forced convection formulas will not show any decreasing trend in stream temperatures or a maximum stagnation temperature as heat is continually added as will the Reynolds method for compressible fluid which will eventually produce choked flow at a certain L/D_e ratio downstream.

Figure 7 shows that the effect on thrust reduction was quite severe for a 2000°F constant wall temperature versus a 2000°F maximum wall temperature; the thrust per square foot was reduced by 18 per cent. For a uniform velocity at the exit of stage 4, a constant change in enthalpy is required. If the neutron flux was such as to produce a series of maximum

wall temperatures from 1600 to 2200°F and with a constant
enthalpy change of 200 BTU per lb imposed, the L/D_e ratio
would vary from 47 to 100. Since all cylinders are desired
to have the same length for nuclear considerations, the hy-
draulic diameters would vary by 47 per cent with decreasing
hydraulic diameters as radial distance is increased. This
diameter variance would still be subject to the limitation
imposed on the hydraulic diameter due to a constant friction
factor.

To increase the thrust which is based on the heat ex-
changer cross-sectional area, each fuel cylinder should oper-
ate at the maximum enthalpy change as shown by Figure 7 and
the thrust would be a weighted average depending on the
frontal area of the heat exchanger. With a constant length
assumed the hydraulic diameter would vary by only 12 per cent.
However, each annulus would be operating at a different veloc-
ity level which may create internal vibration within the ram-
jet pod. With a weighted radial average of 2000°F for the
cylinder temperatures encompassing 7.7 sq ft of heat exchanger
cross-sectional area, from Figure 7 the resultant thrust would
be approximately 9,500 lb at a flight Mach number of 2.5 at
37,500 ft.

With inlet Mach numbers greater than 0.2, the L/D_e ratio
would be substantially reduced. From Reference (2, p.431),
with $M_2 = 0.5$, $f = 0.005$, $T_{0,2} = 1000°R$, $P_{0,2} = 10$ lb/in^2, and
$T_{0,w} = 2000°R$ and 1500°R, choked flow occurred at an L/D_e ratio

of 20 and 35, respectively. To resist the pancaking effect
which may reach the limit for nuclear criticality, the inlet
Mach number appears to have a definite upper limit when heat-
ing is desired.

Conclusion

For the assumed inlet conditions, cylindrical fuel ele-
ments and wall temperatures, the amount of heat transferred
was substantial enough to produce 1,000 to 1,400 pounds of
thrust per sq ft if heat exchanger frontal area with a maximum
wall temperatures range from 1600 to 2200°F at a flight Mach
number of 2.5 and an altitude of 37,500 ft. With a weighted
radial average of 2000°F for the cylinder temperatures encom-
passing 7.7 sq ft of heat exchanger area the resultant thrust
was 9,500 lb.

FUEL ELEMENT CONSIDERATION

Due to the absence of effective moderation within this
nuclear heat exchanger, the unit may be considered as a fast
neutron reactor and as such the restrictions normally imposed
on structural materials by high thermal neutron absorption
may be removed. Whether any structural material now in exist-
ence can be used to contain, protect, and support the fission-
able phase for the high temperatures required is the subject
of the following development and discussion.

Development

The nuclear heat exchanger as shown in Figure 2 incor-
porates thin concentric cylinders which are the solid fission-
able containers. The enriched uranium fuel cores are to re-
main a solid to prevent serious containment problems. The
thin sheets of the fissionable phase are sandwiched between
the inner and outer layers of the non-fissionable structural
metal which predominates in volume so that the alloyed en-
riched uranium fuel sheets are surrounded by a continuous
network of structural metal for strength at high temperatures.

The following are some criteria that were considered for
the selection of fuel elements and structural material:

A. Fuel element criteria

    1. Melting point above 2500°F

    2. Neutron's energy maintained

    3. Mechanical properties similar to the container material during fabrication and high temperature operation.

    4. High thermal conductivity and low specific heat for good heat transfer

    5. Ease of fabrication

B. Container material criteria

    1. High temperature mechanical properties under static and small radial dynamic loads

    2. Resistance to oxidation at high temperatures

    3. High resistance to thermal shock

    4. Neutron energy maintained

    5. Ease of fabrication, rolling, and weldability.

Discussion

The melting point of natural uranium is 2072°F; for the required temperature range of 2000 to 2200°F, the unalloyed uranium would become a liquid and present serious containment problems. In order to increase the melting point, the various binary diagrams of uranium alloys of Saller (8, p.413-414) revealed that a uranium-zirconium system of 20.7 per cent zirconium by atomic weight would have a melting point of 2450°F.

Elements with less than a mass number of 40 were not considered because of the increased slowing down effect on the neutrons.

Zirconium alloys at high temperatures suffer a loss of strength and a loss of corrosion resistance. As reported by Dayton (9, p.460), the strongest alloy tested at 930°F creeps at a rate of 10^{-4} per cent per hour with a stress of only 4000 lb per sq in. Since a thin sheet is sandwiched between two layers of structural material, the loss of strength and corrosion resistance are secondary to the requirement that the fissionable material remain a solid. The coefficient of linear thermal expansion for 20.7 per cent zirconium by weight was not available; however, Dayton (9, p.464) reported a coefficient for pure zirconium at 932°F for the "a" axis of 5.8×10^{-6} while that of pure uranium was anisotropic as shown by Saller (8, p.389). The coefficient of thermal expansion for this particular alloy was not found; however, from Saller (8, p.234) the composition for 20.7 per cent zirconium by weight indicated 3 phase changes for the temperature range up to 2200°F and whether the anisotropic effect of uranium would result in volume changes so severe as to make bonding or cladding impractical was not determined.

The low thermal conductivities of both zirconium and uranium are partially compensated for by low specific heats and the thin sheet effect of high area to volume ratio.

Uranium can be hot rolled without danger of cracking. Whether this particular alloy can be rolled into sheets with thicknesses as small as 0.03 inch was not determined.

The container material for temperatures up to 2200°F presents a considerable problem when restricted to present day material availability. The wrought cobalt-base alloys, such as Haynes Stellite-25, Allegheny-Ludlum Steel Corporation S-590 and S-816, and Westinghouse Electric Corporation Refractaloy 26 and 70, appear to have excellent corrosion resistance up to temperatures as high as 2000°F, Eichen and Jackson (10, p.556), in an oxidizing atmosphere. However, Eichen and Jackson (10, p.539) reported the ultimate strength of Haynes Alloy 25 at 2200°F to be 4,000 lb per sq in. for a sheet 0.042 inch in thickness and annealed at 2200°F. Another major drawback may be the high residual activity in the form of gamma radiation which is characteristic of cobalt-base alloys.

Molybdenum is of interest as a high-temperature material because of its high melting point, 4750°F, high strength and stiffness at elevated temperatures. Northcott (11, p.106) reported creep-rupture strength for wrought arc cast molybdenum, .45 per cent titanium, of 25,000 lb per sq in at 2000°F for 100 hours. The thermal expansion coefficient as reported by Northcott (11, p.26) ranged from 5.1×10^{-6} at 932°F to 7.2×10^{-6} at 3632°F. Thus the thermal expansion of both pure zirconium and molybdenum alloys appear to be very similar.

However, alloying with uranium might alter the thermal expansion characteristic considerably.

Uncoated molybdenum is useless as a material of construction in oxidizing atmospheres above 1000°F. Norden (12, pp.298-304) reported that so far no molybdenum-base alloys have been developed with satisfactory oxidation resistance; however, Hiester et al. (13) reviewed progress made with alloying techniques. Sherwood (14, p.26) stated that molybdenum specimens protected by coatings 0.003 in thick and consisting primarily of molybdenum disilicide have successfully resisted oxidation at 3092°F for more than 1000 hours. However, the coating must be pore-free in order to prevent serious loss of material. Effects of the disilicide coating on heat transfer and thermal cycling were not included.

The high thermal conductivity of molybdenum, .32 cal per sec cm °C, and low specific heat, .061 cal per gm °C, permit it to be heated or cooled rapidly with low resultant stress which give it excellent resistance to thermal shock. The heat transfer characteristics are excellent due to the high thermal conductivity. The neutron moderation effects are small since it has a mass number of 96.

As brought out by Norden (12, p.298) a chief advantage of molybdenum over ceramics, cermets, and some super alloys is the variety of forms and sizes available on a production basis. By the arc-cast methods, sheets from 0.005 to 0.020 in. thick and 36 in. wide are available. Molybdenum has been joined

successfully by spot welding, arc welding, soldering, and brazing but precise controls must be used since excess heating will result in extremely brittle welds.

Conclusion

Molybdenum alloy, 0.45 per cent titanium, with a protective disilicide coating appeared to have the best probability of withstanding temperatures up to 2200°F in an oxidizing atmosphere besides being able to withstand thermal shock and offer near optimum heat-transfer characteristics. The inner fissionable phase of enriched uranium alloyed with 20.7 per cent by weight of zirconium, even though soft and pliable at this temperature range, which could be an advantage as far as the container material is concerned, should expel the heat produced internally due to the high surface to volume ratio. Whether or not the thermal expansion coefficient of the uranium-zirconium would be compatible with molybdenum and that a metallurgical bond would be formed with molybdenum was not ascertained.

NUCLEAR ANALYSIS

The actual heterogeneous reactor configuration as shown
in Figure 2 was treated as a homogeneous unreflected system
using one-group diffusion theory to obtain the critical mass
of uranium. The flattening of flux and reduction of critical
mass by use of a reflector were not considered. The neutron
flux necessary to produce a maximum fuel element temperature
was calculated. The control mechanism necessary to maintain
the flux level was not considered.

Development

The diffusion equation for thermal neutrons for steady
state conditions as developed by Glasstone and Edlund (15,
p.192) is

$$D \nabla^2 \phi (\bar{r}) - \Sigma_a \phi (\bar{r}) + pq (\bar{r}, \tau_{th}) = 0 \quad . \tag{20}$$

For an idealized fast reactor composed of atoms of material
so heavy that neutrons upon colliding rebound without losing
an appreciable amount of energy, the slowing down density term,
$pq (\bar{r}, \tau_{th})$, may be considered negligible. If fast neutrons
occur only at one energy, the source term can be written as

$$S = K \Sigma_a \phi \quad . \tag{21}$$

Using Glasstone and Edlund's (15) treatment the multi-
plication factor may be simplified to

$$K \approx v \left[\frac{\Sigma_f}{\Sigma_a} \right]_{FUEL} \equiv \eta \qquad (22)$$

by assuming that the fast fission factor, the resonance escape
probability, and the fast neutron utilization are essentially
unity. The fast neutron utilization term implies that the
capture of neutrons by material other than the fissionable
phase is negligible. Shapiro (16, p.130) states that the ra-
diative capture cross sections for elements having mass numbers
less than 100 and neutrons numbers less than 60 are not greater
than 50 millibarns. If the fast neutron utilization factor
were not unity, the treatment given by Kaplan (17, p.525) for
thermal neutrons would still apply.

A combination of Equations 20 to 22 yields

$$\nabla^2 \phi \, (\bar{r}) + B^2 \, \phi \, (\bar{r}) = 0 \qquad (23)$$

where $B^2 \equiv \Sigma_a \, (\eta - 1)/D.$ \qquad (24)

For a weak absorber as described by Glasstone and Edlund
(15, pp.92,98), the diffusion coefficient is related to the
transport mean free path by

$$D = \frac{\lambda_t}{3} = \frac{1}{3\lambda_t} \tag{25}$$

where $\lambda_t \equiv \lambda_s (1 - \bar{\mu}_0)$ and $\bar{\mu} = 2/3A$. $\tag{26}$

As a first approximation the macroscopic transport and scattering cross-sections are considered to be essentially equal except in cases where the actual values are known. The atomic masses of the uranium, zirconium, and molybdenum are high enough to make the $\bar{\mu}_0$ term of Equation 26 negligible. As a second approximation the elastic scattering cross section is expected to be equal roughly to the total cross section in the middle energy region of 1 to 500 kev where neutron gamma cross sections are small, Shapiro (16, p.78). The constants used in this analysis are listed in Appendix D with additional refer-ences.

Substitution of Equation 25 into 24 results in

$$B^2 = 3\, \Sigma_t\, \Sigma_a (\eta - 1) \tag{27}$$

The solution to Equation 23 for the buckling in terms of spatial dimensions of a right circular cylinder as developed by Glasstone and Edlund (15, p.213) is

$$B^2 = \left(\frac{2.405}{R}\right)^2 + \left(\frac{\pi}{H}\right)^2 \tag{28}$$

where R and H are the extrapolated radius and height of the cylinder in centimeters.

A combination of Equations 27 and 28 yields

$$3 \, \Sigma_t \, \Sigma_a \, (\eta - 1) = \left(\frac{2.405}{R} \right)^2 + \left(\frac{\pi}{H} \right)^2 \tag{29}$$

Equation 29 is the approximate critical equation for an idealized fast homogeneous unreflected reactor in the form of a right circular cylinder. Appendix D shows the calculations that were used to determine the critical mass of uranium for a right circular cylinder with a physical diameter and length of 42 and 60 in, respectively.

The various component weights which were based on volume fractions with corresponding densities are calculated in Appendix D.

For the flux required to produce the maximum temperature change, the relationship

$$\phi_{max} = \frac{(T_{0.3} - T_{0.2}) \, G \, C_p \, \pi}{4 E \, \Sigma_f t \, (L/D_e)} \tag{30}$$

was used. The result is shown in Appendix D.

Discussion

The length of the heat exchanger was limited to 60 in. because Figure 7 showed that the maximum thrust per sq ft was obtained with an approximate L/D_e ratio of 120. This produced a 0.50 in. hydraulic diameter or a 0.25 in. fuel element spacing

The uranium-zirconium alloy with a composition of 79.3 per cent enriched uranium by weight was selected because of its 2,450°F melting point. A larger percentage of uranium would reduce this melting point which is considered a minimum for the high temperatures desired. The alloy composition was considered a constant and treated as a mixture for volume fractions since the actual density was unknown.

The component volume fractions of the heat exchanger resulted from trial and error thickness selections for the uranium-zirconium and molybdenum alloys which satisfied Equation 29 for a physical diameter and length equal to or less than 42 and 60 in, respectively. Since the physical length was fixed previously for maximum thrust per sq ft, the radius was considered variable.

The nuclear reactor, when treated as a homogeneous un-reflected reactor according to Equation 29, was determined to be critical at a physical diameter of 40 in and a length of 60 in. The large critical volume, 43.6 cu ft, was due to the low macroscopic absorption of uranium, 0.0056 cm^{-1}, which re-sulted indirectly from the 75 per cent volume of air. A de-crease in the volume fraction of uranium would decrease both the total macroscopic absorption and transport cross sections with a resultant increase in radius if the length remained constant.

The weight of enriched, 90 per cent uranium required for the critical volume of 43.6 cu ft was 3,622 lbs. The amount

of zirconium and molybdenum was 960 and 3,470 lbs, respective-
ly, which resulted in a total heat exchanger weight of 8,052
lbs. At current prices of approximately 30 dollars per gram,
50 million dollars would be required for the 90 per cent en-
riched uranium.

The flux that was necessary to generate a maximum wall
temperature of 2200°F with a 0.0315 inch fuel element thick-
ness was 8×10^{14} n per sq cm sec which assumed zero radial
flux depression across the fuel element.

Since the radial flux will follow an approximate cosine
distribution, it is apparent that for an average maximum wall
temperature of 2000°F which was assumed to obtain 9,500 lbs
of thrust with a 7.7 sq ft frontal area, the fuel elements
near the centerline would operate at temperatures exceeding
2200°F. A proposed central control rod and reflector would
tend to flatten the flux; however, the flux envelope resulting
from these effects was not investigated.

The application of the one-energy group diffusion theory
to this analysis was a realistic approximation because the
transport mean free path, 8.7 cm, was small in comparison to
the boundary distance. The extrapolation distance, R-r, is
not generally equal to $0.71 \lambda_t$ for a fast reactor and its
exact value can be obtained only by complicated methods, Glas-
stone (20, p.217). However, as pointed out by Glasstone (20,
p.217), there is probably no point in a fast reactor that is
more than two scattering or transport mean free paths from a

boundary. This statement is supported by the large quantities
of fuel required for the heat exchanger which has a minimum of
11 transport mean free paths in the radial direction.

An intermediate neutron energy reactor may offer the pos-
sibility of reducing the fuel quantity and weight while still
maintaining a large volume fraction of air for compact heat
transfer. The slowing down density term of Equation 20 was
neglected because air, which composed 75 per cent of the heat
exchanger volume, has a negligible moderation effect on neu-
trons. To continue this simplification the material for the
fuel alloy and container was selected from elements with rela-
tively high mass numbers. However, with the proper selection
of lighter materials for the fuel alloy, container and reflec-
tor, the moderation effects may increase to the extent that
this fast reactor would evolve into an intermediate reactor.
It is believed that any trend toward a thermal reactor would
decrease the fuel requirements for the configuration.

Conclusion

From a nuclear aspect this heat exchanger, which was com-
posed by volume of 12.5 per cent alloyed fuel, 12.5 per cent
molybdenum structure, and 75.0 per cent air, was critical at
a diameter and length of 40 and 60 inches, respectively. The
total weight was 8,052 lbs which included 3,622 lbs of enriched

90 per cent uranium.   Approximately 50 million dollars would be required for this amount of uranium.

The flux that was necessary to generate a maximum wall temperature of 2200°F with a fuel element thickness, 0.0315 in. was reasonable at 10^{15}n per sq cm sec.

With cost as a major consideration there is probably no point in a fast reactor more than several scattering or transport mean free paths from a boundary. An intermediate neutron energy reactor may offer the possibility of reducing the fuel quantity and weight for this configuration.

OVER-ALL FEASIBILITY CONCLUSIONS

For an air inlet velocity of $M = 0.2$, a weighted radial average of 2000°F for the maximum cylinder temperature, a frontal area of 7.7 sq ft, a 42 in diameter, and a 60 in length, the amount of heat transferred was substantial enough to produce 9,500 lbs of thrust with a flight Mach number of 2.5 at 37,500 ft.

In order to obtain an average temperature of 2000°F the fissionable material within the thin right circular cylinders had to reach a critical condition. This required 3,622 lbs of enriched 90 per cent uranium with an approximate cost of 50 million dollars. The heterogeneous nuclear heat exchanger was critical with a diameter and length of 40 and 60 in, respectively and a total weight of 8,052 lbs.

The low thrust to weight ratio may be compensated for by the negligible fuel burn up when compared to a turbojet system.

Molybdenum alloy, 0.45 per cent titanium, which was protected with a disilicide coating appeared to have the high temperature properties for the container material. Sandwiched between the molybdenum was an alloy of uranium-zirconium which contained 79.3 per cent uranium by weight. This binary system was selected because of the 2450°F melting point at the above composition. Whether a metallurgical bond could be formed between the molybdenum and fuel alloy was undetermined.

From the above theoretical conclusions and limiting conditions, the over-all feasibility of a compact axial flow nuclear heat exchanger was favorable for thrust, metal availability, and nuclear criticality, borderline for thrust to weight ratio, and unfavorable for the cost of fuel. However, the proposed central control core and peripheral reflector should increase thrust and reduce the cost of fuel because of savings in critical mass.

An intermediate neutron energy reactor may offer the possibility of reducing the fuel requirements. With the proper selection of lighter materials for the fuel alloy, container, and reflector, the moderation effects may increase to the extent that this fast reactor would evolve into an intermediate reactor.

Figure 1. Idealized ramjet in flight at M_0 = 2.5, altitude = 37,500 ft, temperature = 392°R, ambient pressure = 3.09 lb/in^2. Assumed M = 0.2 at station 2.

REFLECTOR

FUEL ELEMENT

AIR

t

CONTROL ROD

D_1

D_2
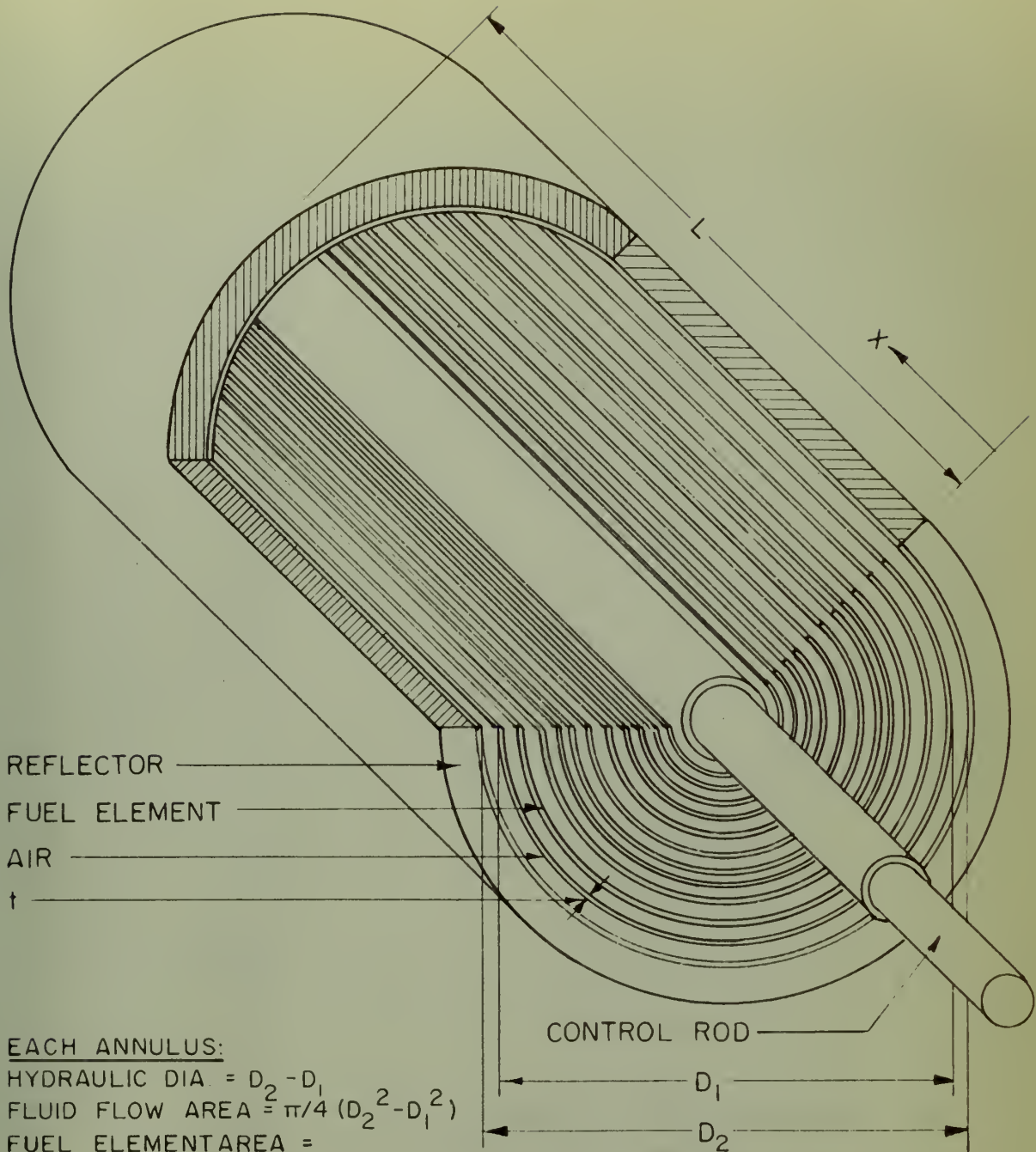
EACH ANNULUS:
HYDRAULIC DIA. $= D_2 - D_1$
FLUID FLOW AREA $= \pi/4\,(D_2^2 - D_1^2)$
FUEL ELEMENT AREA $=$
    $\pi t/2\,(D_1 + D_2)$
HEAT TRANSFER AREA $=$
    $\pi(D_1 + D_2)\,dx$

Figure 2. Nuclear heat exchanger.
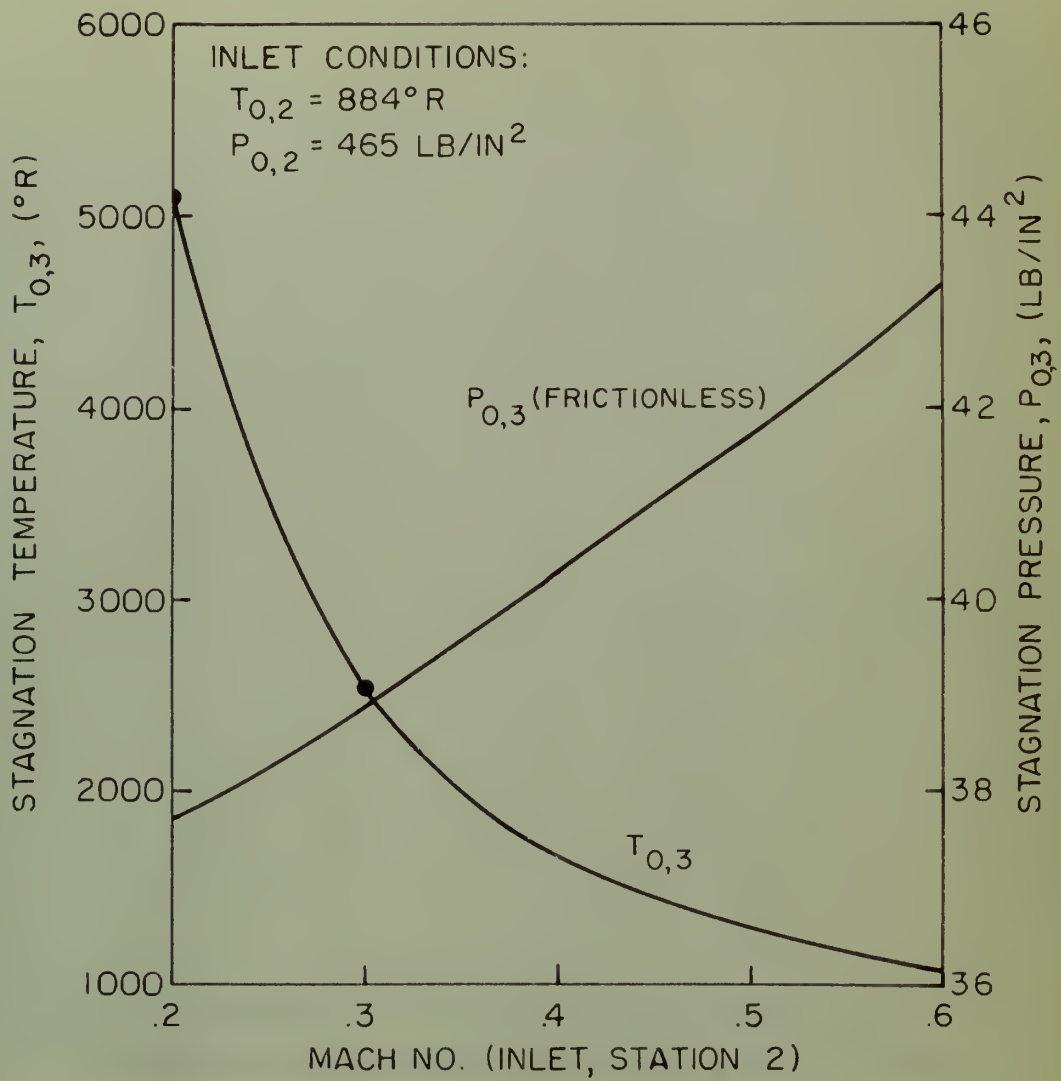
Figure 3. Thermal choking boundaries for a constant area frictionless chamber being heated.
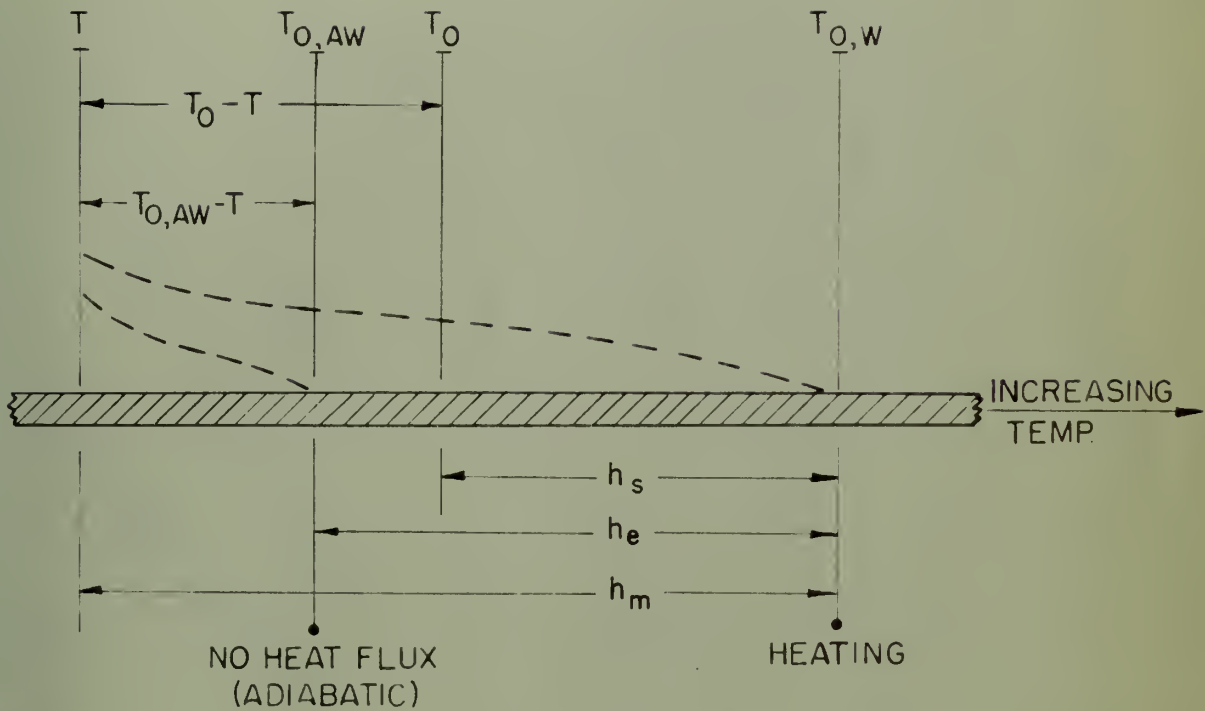
Figure 4. Relationship of various temperatures and heat
transfer coefficients where $T_0 - T = V^2/2gJC_p$
and $N_{RF} = (T_{0,aw} - T)/(T_0 - T)$.
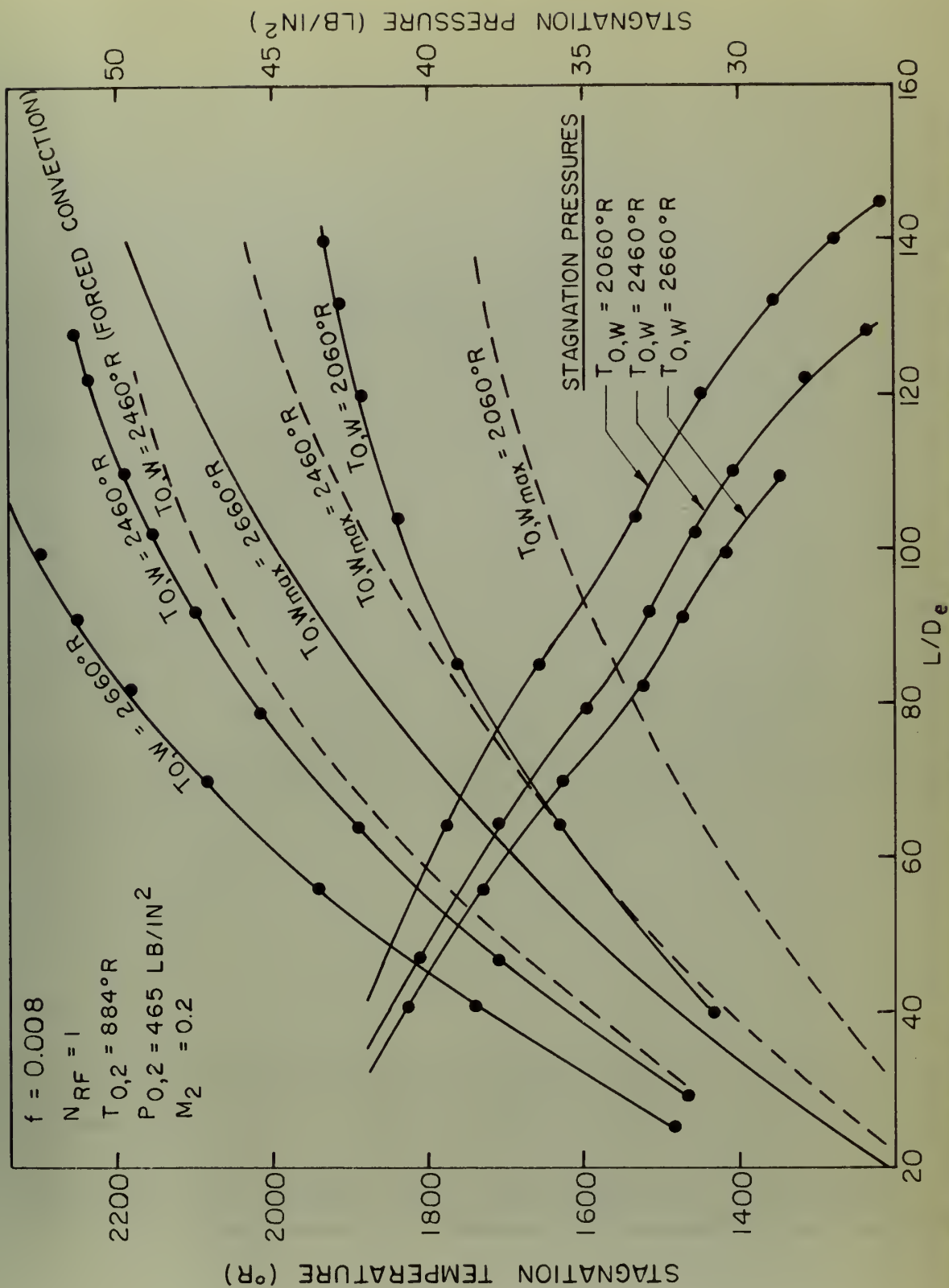
Figure 5. Curves of stagnation temperatures and pressures versus L/D$_e$ ratios.

42
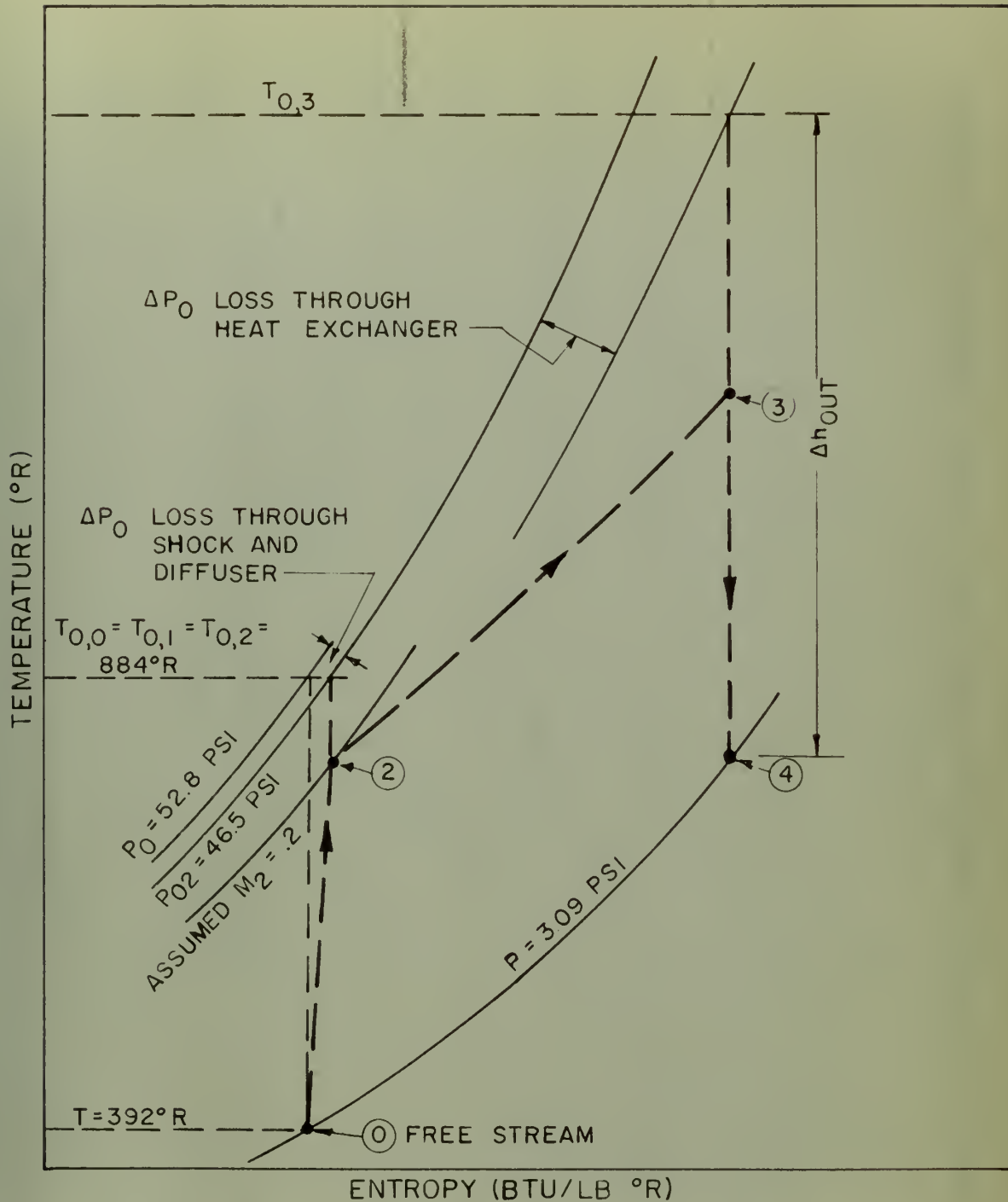
Figure 6. The Brayton cycle for temperature and entropy
conditions for stations corresponding to Figure 1.
Values for dry air are from Reference (7).
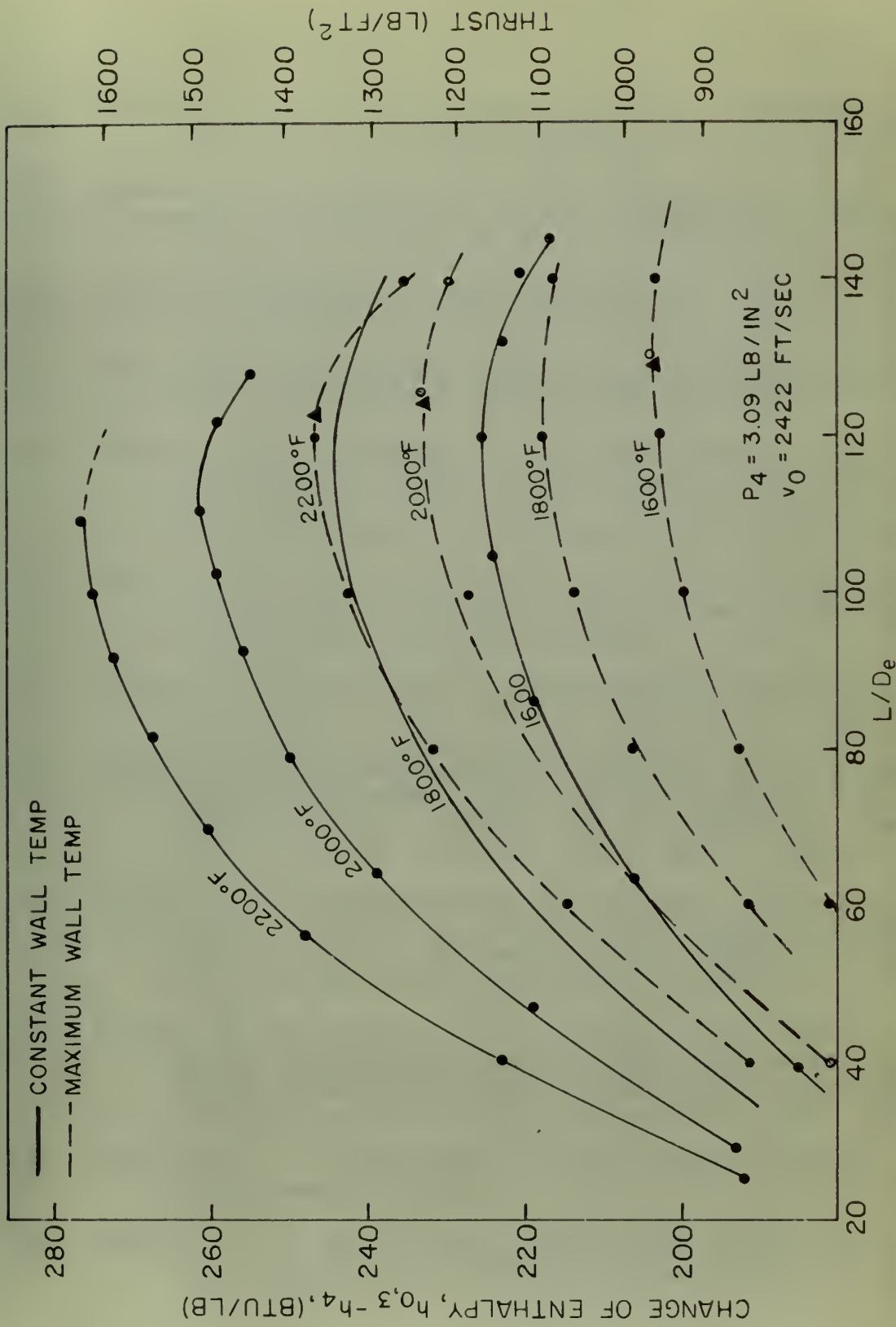
Figure 7. Change of enthalpy and thrust from exit of heat exchanger to exhaust.

LITERATURE CITED

1. Godsey, F. W., Jr. and Young, Lloyd A. Gas Turbines for Aircraft. N. Y., McGraw-Hill Book Co., Inc. (1949).

2. Bureau of Ordnance, U. S. Dept. Navy. Handbook of Super- sonic Aerodynamics. Navord Report 1488 (Vol. 1). Washington, D. C., U. S. Govt. Print. Off. (1950).

3. McAdams, William H. Heat Transmission. 3rd ed. N. Y., McGraw-Hill Book Co., Inc. (1954).

4. Kays, W. M. and London, A. L. Compact Heat Exchangers. Palo Alto, Calif., National Press (1955).

5. McAdams, W. H., Nicolai, L. A., and Keenan, J. H. Meas- urements of Recovery Factors and Coefficients of Heat Transfer in a Tube for Subsonic Flow of Air. Trans. Am. Inst. Chem. Engrs. 42: 907-925. (1946).

6. Cope, W. F. The Friction and Heat Transmission Coef- ficients of Rough Pipes. Proc. Inst. Mech. Engrs. London. 145: 99-105. (1941).

7. Keenan, J. H. and Kaye, J. Thermodynamic Properties of Air. N. Y., John Wiley and Sons, Inc. (1945).

8. Saller, H. A. Uranium and Its Alloys. In U. S. Atomic Energy Commission. The Reactor Handbook. (AECD- 3647). Vol. 3, Section 1. pp. 383-436. Washing- ton, D. C., U. S. Govt. Print. Off. (1955).

9. Dayton, R. W. Zirconium and Its Alloys. In U. S. Atomic Energy Commission. The Reactor Handbook. (AECD- 3647). Vol. 3, Section 1. pp. 459-504. Washington, D. C., U. S. Govt. Print. Off. (1955).

10. Eichen, E. and Jackson, J. H. Cobalt Base Alloys. In U. S. Atomic Energy Commission. The Reactor Hand- book. (AECD-3647) Vol. 3, Section 1. pp. 533-557. Washington, D. C., U. S. Govt. Print. Off. (1955).

11. Northcott, L. Molybdenum. N. Y., Academic Press, Inc. Publishers. (1956).

12. Norden, R. B. Molybdenum Combats High Temperature. Chem. Engr. 64, No. 2: 298-304. (Feb. 1957).

13. Hiester, N. K., Ferguson, F. A. and Fishman, N. High
       Temperature Technology. Chem. Engr. 64, No. 2:
       237-252. (Feb. 1957).

14. Sherwood, E. M. Metals. In Campbell, I. E., Ed. High
       Temperature Technology. pp. 17-28. N. Y., John
       Wiley and Sons, Inc. (1956).

15. Glasstone, Samuel and Edlund, Milton C. The Elements
       of Nuclear Reactor Theory. Princeton, N. J., D.
       Van Nostrand Co., Inc. (1952).

16. Shapiro, Matthew M. Nuclear Physics. In U. S. Atomic
       Energy Commission. The Reactor Handbook. (AECD-
       3645) Vol. 1. pp. 61-364. Washington, D. C.,
       U. S. Govt. Print. Off. (1955).

17. Kaplan, Irving. Nuclear Physics. Cambridge, Mass.,
       Addison-Wesley Publishing Co., Inc. (1955).

18. Murray, Raymond L. Nuclear Reactor Physics. Englewood
       Cliffs, N. J., Prentice Hall, Inc. (1957).

19. Hughes, D. J. and Harvey, J. A. Neutron Cross Sections.
       U. S. Atomic Energy Commission. Brookhaven
       National Laboratory 325. Washington, D. C., U. S.
       Govt. Print. Off. (1955).

20. Glasstone, Samuel. Principles of Nuclear Reactor
       Engineering. Princeton, N. J., D. Van Nostrand
       Co., Inc. (1955).

APPENDIX A

Stepwise Integration for Stagnation Temperature

and Mach Number as a Function of L/D_e Ratio

The procedure used for integration of Equations 13 and 14 are outlined in Reference (2) and are reproduced in part using the following approximations:

1. The integral of dT_0/T_0 may be approximated by $2(T_{0,2} - T_{0,1})/(T_{0,2} + T_{0,1})$.

2. The coefficients of dx/D_e in Equations 13 and 14 are taken at $M_{1,2} = (M_1 + M_2)/2$.

The inlet conditions are as follows:

M_1 = 0.2 $\qquad\qquad$ N_{PR} = 0.664

$T_{0,1}$ = 884°R $\qquad\qquad$ N_{RF} = 0.872

$P_{0,1}$ = 46.5 lb/in^2 $\qquad\qquad$ λ = 1.32

$T_{0,w}$ = 2460°R $\qquad\qquad$ f = 0.008

For a section 2 at a distance $x_2 - x_1$ downstream from section 1, the following computations are carried out.

a. Let $(x_2 - x_1)/D_e$ = 30

b. Estimate M_2 = 0.3, $M_{1,2}$ = 0.25

c. Calculate $2(T_{0,2} - T_{0,1})/(T_{0,2} + T_{0,1})$ from Equation 13.

$$2 \frac{(T_{0,2} - T_{0,1})}{T_{0,2} + T_{0,1}} = \left[\frac{T_{0,W}}{(T_{0,2} + T_{0,1})/2} - 1 + \frac{(1 - N_{PP}) \frac{\gamma-1}{2} M_{1,2}^2}{1 - \frac{\gamma-1}{2} M_{1,2}^2} \right].$$

$$2 \lambda f \quad \frac{x_2 - x_1}{D_e}$$

$$2 \frac{(T_{0,2} - 884)}{T_{0,2} + 884} = \left[\frac{2460}{(T_{0,2} + 884)/2} - 1 + \frac{(1 - .872)(.2)(0625)}{1 + .2(.0625)} \right].$$

$$2(1.32)(.008)(30)$$

$$T_{0,2} = 1640$$

d. Calculate M_2 from Equation 15 and compare with as-
sumed value of M_2

$$M_2^2 - M_1^2 = \frac{.0625(1 + .2 \times .0625)}{(1 - .0625)} \quad 2(.008)(30) \cdot$$

$$\left\{ (1 + 1.4 \times .0625)(1.32) \left[.95 \right] + 2 \times 1.4 \times .0625 \right\}.$$

$$M_2^2 - M_1^2 = 0.0500$$

$$M_2^2 = 0.0500 + 0.0400$$

$$M_2 = 0.3 \quad \text{This agrees with the assumed value.}$$

e. If step d was not successful, repeat the previous
    steps with an improved value of M_2.

f. After convergence is obtained, the process is re-
    peated to find the Mach number at a section 3.

APPENDIX B

Stepwise Integration for Stagnation Temperature

and L/D_e Ratio as a Function of Mach Number

The procedures used for integration of Equations 14 and 17 are outlined in Reference (2). Equation 14 may be integrated approximately over a short interval of Mach number by assuming that the influence coefficients have a constant value corresponding to $(M_1 + M_2)/2$, that the magnitude of T_0 is constant during integration with a value of $(T_{0,1} + T_{0,2})/2$, and that the friction factor is constant. With these approximations and by the substitution of Equation 17 into 14, Equation 14 integrates into

$$M_2{}^2 - M_1{}^2 = 2 \left(\frac{T_{0,2}}{T_{0,1}} - 1\right) \left[\frac{\overline{F}_{T_0}}{\frac{T_{0,2}}{T_{0,1}} + 1} + \frac{2\overline{F}_f}{(\frac{T_{0,W}}{T_{0,1}}) - (\frac{T_{0,2}}{T_{0,1}}) - 1} \right] . \tag{17a}$$

For the same inlet conditions as were given in Appendix A, let

M_2 = 0.24		$M_2{}^2$	= 0.0576
M_1 = 0.20		$M_1{}^2$	= 0.0400
$M_{1,2}$ = 0.22		$M_2{}^2 - M_1{}^2$	= 0.0176

From Reference (2), $\bar{F}_{T_0} = 0.05483$ and $\bar{F}_T = 0.00348$. Equation 17a converged after three attempts to

$$\frac{T_{0,2}}{T_{0,1}} = 1.344 \text{ or } T_{0,2} = 1188°R$$

Equation 14 gave

$$\frac{x_2 - x_1}{D_e} = \frac{1}{2f} \ Ln \ \frac{\dfrac{T_{0,W}}{T_{0,1}} - 1}{\dfrac{T_{0,W}}{T_{0,1}} - \dfrac{T_{0,2}}{T_{0,1}}} = \frac{1}{2(.008)} \ Ln \ \frac{2.785 - 1}{2.785 - 1.344} = 18.85$$

Since both Mach number and stagnation temperatures are known at each section, the following equations were used for computing the remaining properties of the air:

$$\frac{T_2}{T_1} = \frac{T_{0,2}}{T_{0,1}} \frac{(1 + \frac{\gamma-1}{2} M_1^2)}{(1 + \frac{\gamma-1}{2} M_2^2)} \qquad\qquad = 1.34$$

$$\frac{P_2}{P_1} = \frac{M_1}{M_2} \frac{T_2}{T_1} \qquad\qquad = 0.965$$

$$\frac{V_2}{V_1} = \frac{M_2}{M_1} \frac{T_2}{T_1} \qquad\qquad = 1.392$$

$$\frac{\rho_2}{\rho_1} = \frac{P_2}{P_1} \frac{T_1}{T_2} \qquad\qquad = 0.720$$

$$\frac{P_{0,2}}{P_{0,1}} = \frac{P_2}{P_1} \left[\frac{1 + \frac{\gamma-1}{2} M_2^2}{1 + \frac{\gamma-1}{2} M_1^2} \right]^{\frac{\gamma}{\gamma-1}} \qquad = 0.965$$

Tables 1-3 which follow have calculate values for the various properties of air as a function of L/D_e ratios and different constant wall temperatures.

Table 1. Air properties as a function of Mach number for a constant wall temperature of 2660°R and a friction factor of .008

M	T_0 °R	L/D_e	T °R	P lb/in^2	V ft/sec	ρ lb/ft^3	P_0 lb/in^2
0.20	884	0	880	45.1	291	0.1385	46.5
0.24	1192	11.90	1182	43.6	405	0.1000	45.0
0.28	1484	25.50	1466	41.5	524	0.0770	43.0
0.32	1738	40.72	1709	39.2	646	0.0625	40.6
0.36	1939	56.04	1892	36.8	766	0.0528	38.1
0.40	2083	69.94	2020	34.3	881	0.0461	35.6
0.44	2182	81.74	2104	31.8	990	0.0410	33.0
0.48	2252	91.55	2158	29.6	1097	0.0372	31.8
0.52	2299	99.19	2182	27.3	1188	0.0340	30.4
0.60	2356	109.52	2182	23.6	1370	0.0294	28.6

Table 2. Air properties as a function of Mach number for a constant wall temperature of 2460°R and a friction factor of .008

M	T_0 °R	L/D_e	T °R	P lb/in^2	V ft/sec	ρ lb/ft^3	P_0 lb/in^2
0.20	884	0	880	45.1	291	0.1385	46.5
0.24	1184	13.43	1180	43.4	405	0.0998	44.9
0.28	1473	29.32	1462	41.5	527	0.0769	42.9
0.32	1711	46.70	1692	38.9	649	0.0625	40.3
0.36	1891	63.98	1863	36.4	768	0.0533	37.6
0.40	2018	79.33	1970	33.7	878	0.0465	34.8
0.44	2100	92.25	2040	31.2	985	0.0415	32.8
0.48	2155	102.6	2080	28.9	1085	0.0376	31.4
0.52	2192	110.7	2097	26.8	1182	0.0346	30.2
0.60	2236	121.9	2100	23.2	1363	0.0298	27.8
0.70	2258	128.2	2050	19.9	1590	0.0259	25.8

Table 3. Air properties as a function of Mach number for a
constant wall temperature of 2060°R and a friction
factor of .008

M	T_0 °R	L/D_e	T °R	P lb/in^2	P_0 lb/in^2
.20	884	0	880	45.1	46.5
.24	1178	17.95	1160	43.4	44.6
.28	1437	39.75	1411	41.0	42.2
.32	1631	63.55	1592	38.2	39.4
.36	1760	85.95	1711	35.2	36.3
.40	1839	104.7	1775	32.3	33.3
.44	1886	102.0	1811	29.6	31.1
.48	1914	131.9	1830	26.9	28.8
.52	1935	140.6	1830	24.3	26.9
.60	1945	145.6	1800	21.1	25.3

APPENDIX C

Calculation for Outlet Stagnation Temperatures as a
Function of L/D_e Ratios and Maximum Wall Temperatures

With reference to Figure 2, for a heat balance on the
fuel cylinders without axial conduction requires that

$$T_{0,w} - T_0 = \frac{Q_{max}\, t}{2h} \quad \sin\frac{\pi x}{L} \quad . \tag{A}$$

The longitudinal volumetric heat source term is zero when
$x = 0$, or L, which assumes zero extrapolation distance.

Neglecting axial conduction within the fluid and any heat
losses, a heat balance on the air in the annuli requires that

$$T_{0,w} - T_0 = \frac{\rho v C_p D_e}{4h} \quad \frac{dT_0}{dx} \quad . \tag{B}$$

Equating Equations A and B and performing the required
integration results in

$$T_0 - T_{0,2} = \frac{2Q_{max}\, t}{G\, C_p\, \pi} \left(\frac{L}{D_e}\right) \cdot \left[\; 1 - \cos\frac{\pi x}{L} \;\right]. \tag{C}$$

Adding Equations A and C to eliminate the stagnation tem-
perature of the air yields

$$T_{0,w} - T_{0,2} = \frac{Q_{max} \, t}{2h} \quad \sin\frac{\pi x}{L}$$

$$+ \frac{2Q_{max} \, t}{\pi \, G \, C_p} \left(\frac{L}{D_e}\right) \left[1 - \cos\frac{\pi x}{L}\right] \quad . \quad (D)$$

Substitution of Equation 7 with $\lambda = 1$ into Equation D results in

$$T_{0,w} - T_{0,2} = \frac{Q_{max} \, t}{G \, C_p} .$$

$$\left[\frac{1}{f} \sin\frac{\pi x}{L} + \frac{2}{\pi}\left(\frac{L}{D_e}\right) - \frac{2}{\pi}\left(\frac{L}{D_e}\right) \cos\frac{\pi x}{L}\right] .$$

$$(E)$$

From Equation E there appears to be a maximum which repre-sents the highest temperature of the fuel cylinder in the longitudinal direction. The point at which the maximum is at-tained is found by differentiating Equation E and setting the result equal to zero.

$$x_{max} = \frac{L}{\pi} \quad \text{arc tan} \left(-\frac{\pi}{2f} \, \frac{D_e}{L}\right) \quad (F)$$

The maximum wall temperature occurring in the fuel cylin-der can now be obtained by inserting Equation F into equation E. For purposes of computation, it is convenient to represent $\pi x/L$ by the symbol a.

$$a \equiv \pi x/L \quad (G)$$

56

By substituting G into Equation F, results in

$$\tan a_{max} = - \frac{x}{2f} \frac{D_e}{L} \tag{H}$$

Utilizing Equation H, Equation E reduces to

$$T_{0,w_{max}} - T_{0,2} = \frac{2Q_{max} t}{G C_p \pi} \left(\frac{L}{D_e} \right) \left[1 - \sec a_{max} \right] \tag{I}$$

From Equation 17, which was previously derived,

$$\frac{dT_0}{T_{0,w} - T_0} = 2f \frac{dx}{D_e}$$

and introducing Equation A, which was simplified by substituting $h = fGC_p/2$, the following differential equation was derived:

$$dT_0 = \frac{2Q_{max} t}{G C_p D_e} \sin\frac{\pi x}{L} dx \tag{J}$$

Integrating Equation J results in

$$T_{0,3} - T_{0,2} = \frac{4Q_{max} t}{G C_p \pi} \left(\frac{L}{D_e} \right) \tag{K}$$

However, Equation K may be combined with Equation I to eliminate $Q_{max} t$, which results in

$$T_{0,3} - T_{0,2} = 2\,\frac{T_{0,w_{max}} - T_{0,2}}{1 - \sec\alpha_{max}} \tag{18}$$

The magnitude of $T_{0,w_{max}}$ utilized the previously se-
lected wall temperatures. Since $T_{0,2}$ was the given inlet
conditions, α_{max} was computed for various L/D_e ratios result-
ing in $T_{0,3}$ as a function of $T_{0,w_{max}}$ and α_{max}. Table 1 of
Appendix C presents calculated values of $T_{0,3}$ which are shown
in Figure 5.

Table 4. Outlet stagnation temperatures as a function L/D_e
ratios and maximum wall temperatures

L/D_e		40	60	80	100	120	140
$\tan\alpha_{max}$		-4.910	-3.270	-2.450	-1.965	-1.635	-1.405
$\sec\alpha_{max}$		-5.010	-3.420	-2.650	-2.210	-1.920	-1.728
$1-\sec\alpha_{max}$		6.010	4.420	3.650	3.210	2.920	2.728
		$T_{0,2} = 884°R$ and $T_{0,w_{max}} = 2660°R$					
$T_{0,3}$	°R	1475	1688	1858	1990	2101	2184
		$T_{0,2} = 884°R$ and $T_{0,w_{max}} = 2460°R$					
$T_{0,3}$	°R	1408	1597	1748	1865	1964	2038
		$T_{0,2} = 884°R$ and $T_{0,w_{max}} = 2060°R$					
$T_{0,3}$	°R	1275	1415	1529	1616	1689	1745

APPENDIX D

Critical Calculations for a Homogeneous Unreflected Reactor

The effective neutron energy was taken as 0.3 Mev based on flux spectra computed for existing fast reactors by Murray (18, p.69). From the same Reference the following constants were used:

U^{238} : σ_a = 0.18 barns σ_f = 0.0 σ_t = 7.4 barns

U^{235} : σ_a = 1.78 barns σ_f = 1.50 barns σ_t = 7.4 barns

ν = 2.51

From Hughes and Harvey (19) at 0.3 Mev, the total cross sections of the selected reactor materials and air were as follows:

$$Zr : \sigma_T = 9.0 \text{ barns}$$
$$Mo : \sigma_T = 9.0 \text{ barns}$$
$$N : \sigma_T = 4.0 \text{ barns}$$
$$O : \sigma_T = 3.0 \text{ barns}$$

The above total cross sections were considered to be equal approximately to the scattering or transport cross sections.

A 90 per cent enriched uranium mixture by weight produced

$$\frac{235 \ N_5}{238 \ N_8 + 235 \ N_5} = .90 \qquad \text{or} \qquad \frac{N_8}{N_5} = 0.105 \quad .$$

The solution to Equation 22 with the above result yielded

$$\eta = \frac{\sigma_{f,5}}{\sigma_{a,5} + \sigma_{a,8} (N_8/N_5)} = 2.51 \frac{1.50}{1.78 + (.18)(.105)} = 2.09 .$$

Since the alloyed density of the uranium-zirconium system was unknown, the alloy, 79.3 per cent uranium by weight, was treated as a mixture to obtain the following volume fractions:

$$f_{238} = 0.055$$
$$f_{235} = 0.512$$
$$f_{Zr} = 0.432$$

A hydraulic diameter, $D_e = 0.5$ in, was obtained with a selected $L/D_e = 120$ and $L = 60$ in. The following thicknesses were assumed:

Uranium-zirconium alloy: 0.03125 in

Double wall of molybdenum: 0.03125 in

Hydraulic diameter/2: 0.25000 in

Thickness of air space: 0.18750 in

The approximate component volume fractions obtained from the above solidity factors were as follows:

$$f_N = 0.5925$$
$$f_O = 0.1575$$
$$f_{238} = 0.0070$$
$$f_{235} = 0.0640$$
$$f_{Zr} = 0.0540$$
$$f_{Mo} = 0.1250$$

The macroscopic cross sections were computed for each of the above volume fractions which gave for a total

$$\Sigma_t = 0.1183 \text{ cm}^{-1} \quad \text{and} \quad \Sigma_a = 0.0056 \text{ cm}^{-1} \quad .$$

Solution to Equation 27 yielded

$$B^2 = 21.7 \times 10^{-4} \text{ cm}^{-2} \quad .$$

With a physical length equal to 60 in or 152.4 cm and the transport mean free path equal to 8.45 cm, the length including the extrapolation distance was

$$H = h + .71\lambda_t = 152.4 + 6.0 = 158.4 \text{ cm} \quad .$$

The solution to Equation 29 for the critical radius including the extrapolation distance was 56.7 cm; the physical radius was 50.7 cm or 20 in.

Since the total volume was 12.35×10^5 cu cm, the following component weights were determined by using the previously computed volume fractions with corresponding densities:

U^{238}	362 lbs
U^{235}	3260 lbs
Zr	960 lbs
Mo	3470 lbs
Total Weight	8052 lbs

From Equation K, Appendix C, the flux that was necessary
to generate a maximum wall temperature of 2200°F with a fuel
element thickness, 0.0315 in, was obtained with

$$Q_{max} = \frac{(T_{0,3} - T_{0,2})\, G\, C_p\, \pi}{4E\, \Sigma_f\, t\, (L/D_e)}$$

where

$$E = 200 \text{ Mev/fission}$$
$$\Sigma_f = 0.045 \text{ cm}$$
$$Mev = 1.52 \times 10^{-16} \text{ BTU}$$
$$G = 40.4 \text{ lb/ft}^2 \text{ sec}$$
$$C_p = .2671 \text{ BTU/lb °F}$$
$$L/D_e = 120$$
$$T_{0,3} - T_{0,2} = 2101 - 884° \text{ from Figure 5.}$$

The flux obtained from the above equation was 8.25×10^{14} n/
cm^2 sec.